DMD Fast Forward. Published on March 7, 2007 as doi:10.1124/dmd.106.013409
This article has not been copyedited and formatted. The final version may differ from this version.

Pharmacokinetics of ML3403, a 4-pyridinylimidazole-type p38 MAP kinase inhibitor

Bernd Kammerer, Holger Scheible, Wolfgang Albrecht, Christoph H. Gleiter, and Stefan Laufer

University Hospital Tübingen, Department of Clinical Pharmacology (B.K., C.H.G.), Tübingen, Germany;
Eberhard-Karls-University Tübingen, Institute of Pharmacy, Department of Pharmaceutical and Medicinal Chemistry (H.S., S.L.) Tübingen, Germany;
Merckle GmbH (W.A.), Ulm, Germany.

DMD Fast Forward. Published on March 7, 2007 as DOI: 10.1124/dmd.106.013409
This article has not been copyedited and formatted. The final version may differ from this version.

Running title page

Metabolism and Pharmacokinetics of ML3403, a p38 MAP kinase inhibitor

*Correspondence:

Dr. Bernd Kammerer

Address:

@mail: Bernd.Kammerer@uni-tuebingen.de

Fax: +049-7071-29-5035

Document statistics

Number of text pages: 20

Number of tables: 5

Number of figures: 7

Number of references: 25

Number of words in the abstract: 263

Number of words in the introduction: 678

Number of words in the discussion: 353

Abbreviations

ACN acetonitrile; CYP cytochrome P-450 enzyme; ESI electrospray ionization; FA formic acid; GalN D-galactosamine; IL interleukin; IU international unit; k_m Michaelis-Menten constant; LC liquid chromatography; LOQ limit of quantitation; LPS lipopolysaccharide; MAPK mitogen-activated protein kinase; MS/MS tandem mass spectrometry; rcf relative centrifugal force; rCYP recombinant isoenzyme; SD standard deviation; S.E. standard error; SPE solid- phase extraction; SRM selective reaction monitoring; TNF tumour necrosis factor

DMD Fast Forward. Published on March 7, 2007 as DOI: 10.1124/dmd.106.013409
This article has not been copyedited and formatted. The final version may differ from this version.

Abstract

The p38 mitogen-activated protein kinase (MAPK) is a key mediator in cytokine-induced signalling events that are activated in response to a variety of extracellular stimuli such as stress factors, apoptosis and proliferation. Therefore the MAPK family plays an integral role in disease states including oncogenesis, autoimmune diseases and inflammatory processes. Inhibition of these protein kinases represents an attractive strategy for therapeutic intervention. Especially one class of p38 MAP kinase inhibitors – the pyridinyl imidazole derivatives – are intensely investigated by several industrial groups but so far no studies concerning the metabolism of these structurally related substances seem to be available.

The objective of our examinations was the preclinical characterization of ML3403, {4-[5-(4-fluorophenyl)-2-methylsulfanyl-3H-imidazol-4-yl]-pyridin-2-yl}-(1-phenylethyl)-amine a potent inhibitor of p38 MAP kinase – comprising the basic pyridinyl imidazole structure. In human hepatic microsomal incubations, the sulfoxidation to ML3603 and M-sulfone was found to be the predominant metabolic transformation. In addition, oxidative removal of the phenylethyl moiety, pyridine N-oxidation and hydroxylation reactions were observed. Incubations were carried out with hepatic microsomes from various species and with recombinant human CYP isoenzymes, showing that CYP1A2, CYP2C19, CYP2D6 and CYP3A4 are the prominent enzymes in the metabolism of ML3403. Michaelis-Menten kinetics of ML3603 formation by these recombinant isoenzymes showed that CYP3A4 plays a pivotal role in the sulfoxidation reaction. Additionally, pharmacokinetics of ML3403 were evaluated in male and female Wistar rats after oral gavage, showing a fast and high conversion to its active sulfoxide metabolite ML3603. A remarkable gender-specific difference in the systemic exposure to ML3403 and ML3603 was found in rats. No gender-specific difference was detected in incubations with human liver microsomes.

DMD Fast Forward. Published on March 7, 2007 as DOI: 10.1124/dmd.106.013409
This article has not been copyedited and formatted. The final version may differ from this version.

Introduction

p38 MAP kinase (p38) plays a central regulatory role in the biosynthesis of pro-inflammatory cytokines TNF-α, IL-1β and IL-6. Experimental models suggested that p38 inhibition can lead to an improvement or even remission of inflammatory diseases like arthritis (Berenbaum, 2004;Peifer et al., 2006), Crohn's disease (Hommes et al., 2002) or asthma (Barnes, 2004;Newton and Holden, 2003). Consequently, p38 inhibitors have been considered as anti-TNF-α therapeutics which could potentially replace established anti-TNF antibodies or TNF receptors. Many pharmaceutical companies initiated p38 discovery programs (Natarajan and Doherty, 2005;Hynes, Jr. and Leftheri, 2005), but despite the fact that a few candidates have meanwhile reached phase II of clinical development, safety issues appear to represent the main hurdle for a successful development. SB-203580 represents the prototype p38 inhibitor and has been frequently used as benchmark for the evaluation of new compounds (Wagner and Laufer, 2006). SB-203580 and most other p38 inhibitors bind to the enzyme's ATP-binding pocket, which is a highly conserved region of the so-called serine-threonine protein kinases. Thus, the selectivity profile, i.e. the extent of p38 inhibition versus inhibition of other protein kinases, represents a critical feature. Secondly, many imidazoles are known to inhibit cytochrome P-450 enzymes (CYP) which has been associated with liver toxicity.

Publications on p38 MAP kinase inhibitors were usually limited to pharmacological data, mostly describing the *in vitro* potency and its translation into *in vivo* efficacy (Wadsworth et al., 1999). Pharmacokinetic or metabolism data, however, are essentially limited to *in vitro* tests on the inhibition of CYP-isoforms. Detailed characteristics have been published for SB-203580 (Ward et al., 2001) and a follow-up candidate, SB-242235 (Ward et al., 2002a;Ward et al., 2002b). Based on *in vitro* metabolism and pharmacokinetic studies in different animal species, both compounds were characterized as metabolically stable. Excretion data

suggested renal elimination of the unchanged compound as predominant mechanism of disposition. However, the fact that systemic exposure to both drugs increased in an over-proportional manner with ascending doses together with the known affinity of 4-pyridinyl imidazoles to cytochrome P-450 enzymes suggests that metabolic elimination might contribute to their pharmacokinetics.

Several modifications of the diarylimidazoles resulted in an improvement of p38 MAP kinase selectivity and a reduction of CYP-inhibition (Laufer et al., 2003). However, keeping in mind that minor modifications of the chemical structure could have a dramatic impact on the protein kinase selectivity, metabolism studies with protein kinase inhibitors are of great importance. ML3403 (Figure 1) belongs to the second generation of diarylimidazole-type p38 MAP kinase inhibitors (Laufer et al., 2003). The potency towards p38α is approximately twofold when compared to SB-203580 and in Balb/c mice, the LPS/GalN-induced release of TNF-α was completely inhibited when doses of 30 and 100 mg/kg body weight ML3403 were orally administered 1 h before the LPS/GalN-challenge. Preliminary *in vitro* metabolism studies demonstrated a rapid oxidation of the sulfanyl group to the corresponding sulfoxide, denominated as ML3603. The *in vitro* pharmacological profile of the metabolite was similar to that of the parent drug, but with a slightly reduced CYP-inhibition potency (inhibition of CYPs 1A2; 2C9; 2C19; 2D6; 3A4 @ 10 µM by ML3403/Ml3603 [%] 68/52; 76/60; 66/54; 33/23; 85/61).

Besides ML3603, additional metabolites were detected. Detailed analyses confirmed that ML3403 and ML3603 were also subject to pyridine-N-oxidation and dealkylation. Based on the identification of metabolites, a biotransformation pathway has been proposed. As these initial studies were carried out with liver microsomes from CD-1 mice, the relevance of the identified metabolites remained unknown. Therefore, to evaluate the importance of the metabolism of ML3403, *in vitro* metabolism studies with liver microsomes from different

species, i.e. mouse, rat, primate and humans, were performed. Additionally, the intrinsic clearance of ML3403 was determined in liver microsomes, and human recombinant CYP-isoforms involved in the biotransformation were identified. In a pilot pharmacokinetic study, ML3403 was administered to male and female Wistar rats. Plasma samples were used for quantification of the parent drug and the main metabolite ML3603 as well as for detection of additional metabolites. It could be demonstrated that metabolites formed in Wistar rats *in vivo* are identical to those obtained in *in vitro* studies.

DMD Fast Forward. Published on March 7, 2007 as DOI: 10.1124/dmd.106.013409
This article has not been copyedited and formatted. The final version may differ from this version.

Materials and Methods

Reagents

ML3403, {4-[5-(4-fluorophenyl)-2-methylsulfanyl-3H-imidazol-4-yl]-pyridin-2-yl}-(1-phenylethyl)-amine, ML3603, {4-[5-(4-fluorophenyl)-2-methylsulfinyl-3H-imidazol-4-yl]-pyridin-2-yl}-(1-phenylethyl)-amine, M-sulfone, {4-[5-(4-fluorophenyl)-2-methylsulfonyl-3H-imidazol-4-yl]-pyridin-2-yl}-(1-phenylethyl)-amine, and the internal standards ML3435, {4-[5-(4-fluorophenyl)-2-methylsulfanyl-3H-imidazol-4-yl]-pyridin-2-yl}-phenyl-amine, and ML3596, {4-[5-(4-fluorophenyl)-2-methylsulfinyl-3H-imidazol-4-yl]-pyridin-2-yl}-phenyl-amine) were synthesized in the Department of Drug Research, Merckle GmbH (Ulm, Germany).

Acetonitrile (ACN) and methanol LiChrosolv hypergrade, formic acid (FA) p.a. were purchased from VWR (Darmstadt, Germany).

$NADP^+$ sodium salt, Trizma base and Trizma HCl, magnesium chloride-hexahydrate, glucose-6-phosphate sodium salt, glucose-6-phosphate dehydrogenase from yeast were purchased from Sigma-Aldrich Chemie GmbH (Muenchen, Germany), human plasma of different donors was kindly provided by Blutbank / UKT (University Hospital Tuebingen, Germany).

Water was used from an in-house bi-distillation device (Department of Pharmaceutical Biology, University of Tuebingen, Germany).

In vitro metabolism studies

Liver microsomes of CD-1 mice (MLM), rat (RLM), cynomolgus monkey (CMLM) and human (HLM) prepared by the Department of Drug Research Merckle GmbH (Ulm,

DMD Fast Forward. Published on March 7, 2007 as DOI: 10.1124/dmd.106.013409
This article has not been copyedited and formatted. The final version may differ from this version.

Germany) were used. These liver microsomes were characterised in protein and cytochrome P-450 content.

Baculovirus cDNA-expressed isoenzymes (Supersomes) of CYP1A2 with P-450 reductase, CYP2C8 with P450 reductase/cytochrome b_5, CYP2C9*1 (Arg_{144}) with P-450 reductase/cytochrome b_5, CYP2C19 with P-450 reductase/cytochrome b_5, CYP2D6*1 with P-450 reductase, CYP3A4 with P-450 reductase/cytochrome b_5, FMO3, Supermix, P-450 reductase/cytochrome b_5 insect cell control, insect cell control and pooled male and female RLM and HLM were purchased from Gentest (Woburn, MA).

All incubations (final total volume: 500 µl) were made in the presence of an NADPH-regenerating system consisting of glucose-6-phosphate (5 mM), glucose-6-phosphate dehydrogenase (1 IU/ml) and $NADP^+$ (1 mM). ML3403 (2 µM), NADPH re-generating system and $MgCl_2$ x 6 H_2O (1.6 mM) in 0.1 M Tris buffer (pH 7.4) were pre-incubated for 10 min in a shaking water bath at 37°C, 50 rpm and the reaction was started by addition of microsomes (0.5 mg protein/ml or 25 pmol CYP/mg). To follow the time course of metabolism, at different time points (0, 10, 30, 60 and 90 min), 50 µl aliquots were withdrawn and transferred into a ice-cooled vial containg 150 µl H_2O, 150 µl ACN and 50 µl internal standard solution (ML3435 and ML3596 in concentrations of 100 ng/ml each). The samples were vortexed for 15 sec and centrifuged (19800 *rcf*/4°C/10 min). The supernatant was directly used for analysis. All incubations were conducted in triplicates; average mean values of these incubations are shown in the figures. In all incubations it was avoided to exceed a limit of 1% organic solvent (Chauret et al., 1998;Busby, Jr. et al., 1999).

Clearance predictions by substrate depletion approach (*in vitro* t½ method)

For microsomal incubations of different species, the substrate depletion approach was used to calculate the *in vitro* intrinsic clearance (Obach et al., 1997). ML3403 was incubated for 90

DMD Fast Forward. Published on March 7, 2007 as DOI: 10.1124/dmd.106.013409
This article has not been copyedited and formatted. The final version may differ from this version.

min with the same protein content in each of the different species liver microsomes. Five aliquots were drawn at time points 0, 10, 30, 60 and 90 min as described above. ML3403 concentrations were then determined by the online SPE-LC-MS/MS method and normalized to the amount of ML3403 at t = 0 min. The logarithm of the percentage remaining versus time was fitted by least-squares linear regression of at least 4 time points. If substrate decline demonstrated nonlinearity, only those initial time points where log-linearity was observed were used to determine the depletion rate constant. The *in vitro* t½ for the microsomes was used to calculate CL_{int} for microsomal incubations:

$$CL_{\text{int microsomes}} = \frac{\ln 2 * liver\,weight * 45\,mg\,microsomes\,per\,g\,liver}{in\,vitro\ t_{1/2} * microsomal\ \ protein\,concentration\,in\,incubation} \qquad (1)$$

Liver weights and the standard value of 45 mg microsomal protein-content per gram liver of mouse, rat, monkey and human were taken from Davies and Morris and Houston (Davies and Morris, 1993; Houston, 1994).

In vivo clearance $CL_{p\ \text{in-vivo}}$ was calculated from *in vitro* intrinsic clearance $CL_{\text{int microsomes}}$ using the well-stirred and parallel-tube model (Pang and Rowland, 1977), where Q is the hepatic blood flow (Davies and Morris, 1993) and f_u represents the free fraction in blood (here considered as 1).

Well-stirred model:

$$CL_p = \frac{Q * f_u * CL_{\text{int}\ microsomes}}{Q + f_u * CL_{\text{int}\ microsomes}} \qquad (2)$$

Parallel-tube model:

$$CL_p = Q * \left(1 - e^{\frac{-CL_{\text{int}\ microsomes} * f_u}{Q}}\right) \qquad (3)$$

DMD Fast Forward. Published on March 7, 2007 as DOI: 10.1124/dmd.106.013409
This article has not been copyedited and formatted. The final version may differ from this version.

Determination of kinetic parameters for the sulfoxidation of ML3403 to ML3603

k_m and V_{max} were determined in pooled female and male human liver microsomes, baculovirus cDNA-expressed isoenzymes (Supersomes) of CYP1A2 with P-450 reductase, CYP2C19 with P-450 reductase/cytochrome b_5, CYP2D6*1 with P-450 reductase, CYP3A4 with P-450 reductase/cytochrome b_5. The substrate concentrations ranged from 0.1 µM to 50 µM. The protein content and time linearity was proven in proceeding analysis: The protein content determined, was 0.03 mg/ml for HLM and, the cytochrome P-450 content was 0.5 pmol/ml for cDNA-expressed isoenzymes. Incubations were conducted in a total volume of 250 µl, for an incubation time of 10 min and performed in duplicates for the liver microsomes or triplicates for the rCYP. Data reported are averages ± standard errors of the determinations. Estimation of the enzyme kinetic parameters was made by fitting to the Michaelis-Menten equation by best-fit nonlinear regression using the Enzyme Kinetics Module 1.1/Sigmaplot 8.02a software (Systat Software Inc., Richmond CA).

Goodness of fit was assessed by calculation of correlation coefficient (R^2) and Akaike information criterion (AIC) and visual examination of the data.

The microsomal and the CYP2D6 metabolite appearance data were best described using the Substrate Inhibition Kinetic model (Tracy and Hummel, 2004).

$$v = \frac{V_{max}}{1 + \frac{k_m}{[S]} + \frac{[S]}{k_i}} \qquad (4)$$

All other Supersomes metabolite appearance data were modelled with the typical Michaelis-Menten equation

$$v = \frac{V_{max} * [S]}{k_m + [S]} \qquad (5)$$

The “total normalized rate” (TNR) of each recombinant isoenzyme is calculated based on the method described by Rodrigues (Rodrigues, 1999).

Pharmacokinetic studies in Wistar rats

The animal experimental part of this study was performed at Charles River Wiga Deutschland GmbH (Kisslegg, Germany). ML3403 was administered to eight female and male Wistar rats with a single oral gavage (p.o.) dose of 30 mg/kg body weight. The drug formulation was prepared by grinding 60 mg of ML3403 in a mortar; a small amount of 1% methyl cellulose (MC) was added until a smooth paste was obtained. The paste was transferred into a graduated flask and made up with 1% MC to a volume of 10 ml. A dose of 5 ml/kg was administered with continuous stirring of the suspension.

For blood sampling, groups were allocated to schedules A or B. In schedule A, five samples were taken at time points 0 h (pre-dose), 0.5 h, 2.0 h, 6.0 h and 11.0 h after dosing in animals 1 - 4. In schedule B, five samples were taken at time points 0 h, 1.0 h, 4.0 h, 9.0 h and 24.0 h after dosing in animals 5 - 8.

Blood samples of about 300 µl were drawn from the vena jugularis through an indwelling catheter into lithium-heparinised Eppendorf tubes. The catheter tube was removed 1 to 2 cm out of the subcutaneous spinal pouch and rinsed with 0.2 to 0.3 ml heparin-glucose solution. The blood samples were then withdrawn with a 1 ml-syringe and a prepared pipette tip. The catheter tube was rinsed again and pushed back into the subcutaneous spinal pouch.

Blood samples were centrifuged for 10 min at 3000 rpm at 10°C, and plasma (about 150 µl) was transferred into Eppendorf tubes and stored at -80°C.

Pharmacokinetic data were evaluated according to a non-compartmental pharmacokinetic model using the software WinNonlin 4.0.1 (Pharsight Corp., Mountain View CA).

Online LC-SPE-MS/MS analysis of plasma samples

DMD Fast Forward. Published on March 7, 2007 as DOI: 10.1124/dmd.106.013409
This article has not been copyedited and formatted. The final version may differ from this version.

For quantitative analysis of ML3403 and ML3603 in plasma samples, a fast and simple method was developed. The method is based on an online solid-phase extraction (SPE) in the first dimension to remove polar matrix elements coupled to a reversed-phase chromatography in the second dimension with a sensitive triple quadrupole mass spectrometric (MS) detection in the selective reaction monitoring (SRM) mode. The method is capable to analyse ML3403 and ML3603 with two internal standards in 5 min without time-consuming offline extraction steps.

Plasma samples were thawed at room temperature. An aliquot of 50 µl was drawn and mixed with 50 µl of internal standard solution containing 100 ng/ml ML3435 and ML3596 each. For protein precipitation, 300 µl ACN was added and the sample thoroughly vortexed for 15 seconds. After centrifugation at 10°C with 19800 *rcf*, the supernatant was transferred into HPLC vials and directly used for analysis.

Nine standard solutions (2.5, 5, 10, 50, 500, 1000 and 2500 ng/ml) and three quality controls (3.75, 75 and 1250 ng/ml) were prepared by spiking human plasma of different donors. Blank human plasma and pre-dose rat plasma were used to confirm the specificity of the method.

Online SPE was performed on an Oasis HLB cartridge (Waters Eschborn, Germany) with an isocratic clean-up flow of H_2O/ACN/FA (98/2/0.1) at 2.5 ml/min. For the chromatographic separation, a GROM 120 SIL-ODS 4 HE (50*2 mm, 5 µm) with a precolumn of the same material (GROM Rottenburg, Germany) was used with a linear binary gradient of solvent A (water/0.1% FA) and B (ACN/0.1% FA) at a flow rate of 500 µl/min during 5 min, beginning with 20% B for 0.5 min and an increase to 100% B at 4.5 min till to the end. After each injection, the SPE cartridge was regenerated with an injection of 100 µl MeOH/ACN/H_20/FA (10/10/4/0.1 V/V/V/V) within 1.5 min. The gradient for the wash step was 100% B for 0.5 min, changing to 20% B in 0.05 min, holding to the end. The detection was performed on a TSQ Quantum triple quadrupole MS (Thermo Finnigan, San Jose CA) in the electrospray

ionization (ESI)-positive SRM mode. This method was validated in respect to matrix effects, linearity, selectivity, intra- and interday precision and accuracy. The linear range of the method extends from 2.5 ng/ml (LOQ) to 2500 ng/ml. All metabolite areas of the SRM traces were related to the area of the 100 ng/ml internal standard ML3596 and multiplied with 100. This procedure also served for semi-quantification of metabolites for which reference material was not available.

Screening of metabolites by LC-MS/MS analysis

The chromatographic separation was performed on a Grom 120 SIL-ODS 4 HE (150*2 mm, 5 µm) with a precolumn of the same material. A binary gradient of 35 min with solvents A and B (vide supra) at a flow rate of 200 µl/min was used. The initial composition with 5% B was held for 7 min, followed by linear gradients up to 30% B in 3 min, up to 40% in 10 min, up to 50% in 4 min and up to 95% in 3 min, holding for 3 min, changing to 5% B in 0.1 min and re-equilibrating until end.

Detection was performed either on a Surveyor PDA (Thermo Finnigan, San Jose CA) at 320 nm and on the TSQ Quantum triple quadrupole MS in ESI positive mode. Spray voltage was set at 3.2 kV and the heated capillary operated at 320°C, Sheath gas and Aux gas flow rate worked at 40/10 arbitrary units.

Eluates from the first and the last 8 minutes were diverted to waste to prevent contamination of the interface of the mass spectrometer by matrix components.

DMD Fast Forward. Published on March 7, 2007 as DOI: 10.1124/dmd.106.013409
This article has not been copyedited and formatted. The final version may differ from this version.

Results

Metabolic stability of ML3403 in different species: Mouse, rat, cynomolgus monkey and human liver microsomes

To investigate the metabolic stability of ML3403 in vitro, biotransformations with liver microsomes from different animal species and humans were performed. To compare the rates of substrate degradation, the microsomal protein content was standardized (0.5 mg/ml). Immediately after initiation of the reaction as well as after 10, 30, 60 and 90 min, aliquots were withdrawn and prepared for LC-MS/MS analysis. In all incubations, more than 90% of the substrate ML3403 was degraded within the incubation period of 90 min. The most efficient biotransformation were observed with microsomes from cynomolgus monkeys and CD-1 mice with a >90 % degradation within 30 and 10 min, respectively.

The main metabolite of ML3403 was the corresponding sulfoxide, ML3603. Kinetic analyses demonstrated that ML3603 reached a concentration maximum between 5 and 30 min. Further degradation led to the formation of the corresponding N-oxide (M-437-pyr), M-sulfone and the dealkylation product M-317 (Figure 2). All of the identified metabolites could be found in different amounts in all of the examined species liver microsomes. In comparison to the other species, microsomes from cynomolgus monkey converted ML3403 much faster into the pyridine N-oxide metabolites M-421-pyr and M-437-pyr.

In vitro metabolism in baculovirus-expressed human CYP isoenzymes

To identify the enzymes involved in the biotransformation of ML3403, incubations with six cytochrome P450-isoenzymes (CYP1A2, CYP2C8, CYP2C9, CYP2C19, CYP2D6 and CYP3A4) were performed. For the evaluation of the concentration time profiles of substrate and metabolites, a mixture of the six most abundant individual baculovirus cDNA-expressed

cytochrome P-450 isoenzymes (Supermix) was compared with the time profiles produced by human liver microsomes (HLM).

To this end individual Supersomes containing CYP1A2, CYP2C8, CYP2C9, CYP2C19, CYP2D6 and CYP3A4 were combined to simulate the average relative enzyme activities described for HLM. In this Supermix assay, the rate of degradation of ML3403 as well as the metabolite profile was similar to that observed with HLM. Thereafter, the potential involvement of flavin monooxygenase isoform 3 (FMO3) in the metabolism of ML3403 was tested. Incubations without NADPH and with cytochrome P-450 reductase/b5 without CYP enzymes served for excluding non-enzymatic metabolite formation.

Incubations with FMO3, with control microsomes and without NADPH did not lead to an increase in any of the metabolites. Incubations with microsomes which were heated to 45°C for 5 min to inactivate FMOs showed no difference to incubations with freshly thawed microsomes. This demonstrates that the cytochrome P-450 enzyme system is responsible for the phase I-biotransformation of ML3403.

In the sulfoxidation reaction to ML3603 and further oxidation to M-sulfone, four cytochrome isoenzymes are primarily involved: CYP1A2, CYP2C19, CYP2D6 and CYP3A4. Figure 3 shows the percentage of ML3603 and M-sulfone formation after an incubation of 10 min in relation to the amount of ML3403 in the control incubation.

Apart from the predominant S-oxidation, the removal of the phenylethyl group leading to the metabolite M-301 and oxidation of the pyridine nitrogen producing M-421-pyr represent relevant biotransformations. Incubations with isolated CYP-isoforms demonstrated that these reactions are catalysed by CYP3A4. Subsequent S-oxidation resulted in the formation of M-317 and M-437-pyr, respectively (Figure 2). In incubations of ML3403 with 2C19, a hydroxylation of the phenylethyl moiety was found, the exact position of the introduced hydroxyl group, however, could not be localized.

DMD Fast Forward. Published on March 7, 2007 as DOI: 10.1124/dmd.106.013409
This article has not been copyedited and formatted. The final version may differ from this version.

Involvement of different rCYPs of the sulfoxidation reaction by "total normalized rates" (%TNR)

Michaelis-Menten kinetics of ML3403-degradation was determined for the CYP-isoforms 1A2, 2C19, 2D6 and 3A4 which are predominantly responsible for S-oxidation (Figure 5). The kinetic constants km and V_{max} of each CYP-isoform were derived by non-linear regression of v/concentration data pairs and used for calculation of their contribution *in vivo* using the total normalized rates (TNR) approach. In the sulfoxidation reaction to ML3603, CYP3A4 was the major isoenzyme calculated to contribute 50% to the reaction, followed by CYP1A2 with 32% and CYP2D6 with about 16% (Table 2).

***In vitro* metabolism in female and male rat and human liver microsomes**

To examine gender-specific differences, incubations of male and female pooled RLM were compared to incubations with male and female pooled HLM. The time profile of the RLM showed clear-cut differences in metabolite formation rates. Male RLM produced ML3603 and M-sulfone faster compared to female RLM (Figure 3). In HLM gender differences were much less distinct, especially when considering the higher CYP enzyme activity of the female microsomes. Michaelis-Menten kinetic measurements in pooled male and female HLM resulted in k_m-values for ML3403 sulfoxidation that did not differ significantly (Figure 5).

Intrinsic clearance estimation in different species by substrate depletion approach

For the prediction of *in vivo* intrinsic clearance by the substrate depletion approach, the disappearance rate of ML3403 was measured in microsomes from different species at a low substrate concentration of 2 µM. The determined *in vitro* half-time ($t_{½}$) was very fast in mouse ($t_{½}$=6 min) and rat ($t_{½}$=11 min), whereas a strong difference between female ($t_{½}$=166

min) and male ($t_{½}$=9 min) rats was observed. The calculated plasma clearances (C_p) using the well-stirred model were slightly lower than the C_p-values using the parallel-tube model. A compilation of the parameters is given in Table 1.

Pharmacokinetics in rat

To investigate the rate and extent of systemic exposure of the parent drug ML3403 and its main metabolite ML3603 in vivo, a dose of 30 mg/kg was orally administered to male and female Wistar rats. A dose formulation suitable for intravenous administration was not available. Plasma concentrations of ML3403 and ML3603 were determined by LC-MS/MS and pharmacokinetic parameters were derived by non-compartmental analysis of mean plasma concentration / time profiles (Figure 6).

The individual and derived mean concentration/time profiles reflect a rapid absorption of the parent drug and rapid appearance of the metabolite. The concentrations of the metabolite ML3603 were substantially higher than those of ML3403. Monophasic elimination kinetics were observed for both compounds.

In female animals, concentration/time profiles could be followed for 24 hours. In contrast, plasma concentrations in male rats were below the LLQ of 2.5 ng/ml at 24 h post-dose.

The kinetic parameters of animals 1 - 4 were derived from data measured at 0 - 11 h and for animals 5 - 8 at 0 - 24 h. Therefore, AUC_{0-t} values determined for animals 1 - 4 cannot be directly compared with those of animals 5 - 8. To allow the calculation of the total exposure towards ML3403 plus ML3603, the parameters were converted into µM for C_{max} and µM*h for AUC_{0-t}.

Calculated pharmacokinetic parameters for ML3403 and ML3603 based on mean concentration/time profiles are given in Table 4 and the calculated ratios female/male of the parameters C_{max} and AUC are given in Table 5.

DMD Fast Forward. Published on March 7, 2007 as DOI: 10.1124/dmd.106.013409
This article has not been copyedited and formatted. The final version may differ from this version.

Identification of phase I metabolites in Wistar rats

Besides the predominant sulfoxidated metabolite ML3603, seven more metabolites were found in liver microsomal incubations of different species. These metabolites were named M-301, M-317, M-333, M-421-pyr, M-437-121, M-sulfone and M-437-pyr (Figure 2). The structural elucidation was carried out by MS/MS- and in-source CID MS^3-fragmentation pattern, LC-cryo NMR-MS coupling and comparison of the retention times as described in our previous work (Kammerer et al., 2007). All these metabolites could be identified in plasma samples of Wistar rats after oral gavage of ML3403.

Identification of phase II metabolites in Wistar rats

Besides the major metabolites, two dominant peaks could be detected in rat plasma samples with protonated molecule peaks at 331 m/z (M-331) and 345 m/z (M-345), respectively. The MS/MS-spectra of M-317 versus M-331 and M-345 revealed characteristic shifts of 14 *Da* and 28 *Da* (Figure 7). The proposed fragment ions confirm the suggested structures of the two phase II-metabolites as N-methylated derivatives of the sulfoxide from which the phenylethyl group is removed (M-317).

Additionally two minor unknown peaks with a $[M+H]^+$ at 359 Da (M-359) and 361 Da (M-361) could be identified in the chromatogram. According to MS/MS- and in-source pseudo MS^3-spectra, the two metabolites could be characterized as two more phase-II metabolites. The chemical structure of M-359 could be assigned as the acetyl-conjugated derivative (+ 42 *Da*) of M-317 with a characteristic loss of CH_3CO (Levsen, et al, 2005) in MS and M-361 was identified as the dimethyl-conjugated metabolite of M-333 (+ 28 *Da*). The structures and characteristics of all identified *in vivo* metabolites are given in Figure 2 and Table 5.

DMD Fast Forward. Published on March 7, 2007 as DOI: 10.1124/dmd.106.013409
This article has not been copyedited and formatted. The final version may differ from this version.

Discussion

In the present study, the metabolism of ML3403, a second-generation p38 MAP kinase inhibitor, was investigated. Microsomal incubations revealed the isoenzymes CYP1A2, CYP2C19, CYP2D6 and CYP3A4 as key enzymes in the metabolism of ML3403. Several metabolites including the pyridine N-oxides (M-421-pyr and M-437-pyr) and the sulfone (M-sulfone) are mainly produced by CYP3A4.

CYP3A4 was identified also as the main contributor for mediating the N-dealkylation of the phenylethyl moiety. The resulting primary amine undergoes conjugation reactions in rats: N-methylation, N-dimethylation and N-acetylation.

In an extension of the *in vitro* study, the *in vivo* pharmacokinetics of ML3403 in Wistar rats were examined. After oral gavage, ML3403 showed a fast and high turnover into its active sulfoxide metabolite ML3603 comparable to the *in vitro* findings. In the plasma samples, the t_{max} values of ML3403 and ML3603 were identical (1h post dose). The fast metabolic conversion *in vitro* and the high involvement of the CYP isoenzyme 3A4 – known to be present also in the small intestine (Kolars et al., 1992;Hall et al., 1999) – are suggestive of a first-pass metabolism.

The calculated pharmacokinetic data clearly demonstrate a substantially higher systemic exposure of female animals to both the parent drug ML3403 and the sulfoxide metabolite ML3603. However, the systemic elimination of both compounds shows highly similar kinetics in male and female animals. Therefore, gender-specific differences of processes responsible for systemic elimination are unlikely (Ripp et al., 1999). The influence of gender-specific metabolism in rat was shown in incubations with male and female RLM. Male rats showed a faster conversion into all metabolites; particularly the oxidative removal of the phenylethyl moiety proceeded faster than in female rats. Besides gender-specific mechanisms

during drug absorption and/or pre-systemic elimination, this could be a reason for the higher systemic exposure to ML3603 in female rats. For HLM gender-specific differences could not be shown *in vitro.*

In conclusion, all *in vitro* metabolites could be detected in rat plasma samples; 4 new conjugated *in vivo* metabolites (M-331, M-345, M-359 and M-361) were described. The main oxidative pathway is predominantly catalysed by CYP3A4, CYP1A2 and CYP2D6, for the desalkylation and pyridine N-oxidation, CYP3A4 is nearly solely responsible.

Acknowledgments

The authors wish to acknowledge the support of the Pharsight Corp., (Mountain View CA) providing us with an academic free license of the WinNonlin 4.0.1 software suite.

DMD Fast Forward. Published on March 7, 2007 as DOI: 10.1124/dmd.106.013409
This article has not been copyedited and formatted. The final version may differ from this version.

References

Barnes PJ (2004) New Drugs for Asthma. *Nat Rev Drug Discov* **3**:831-844.

Berenbaum F (2004) Signaling Transduction: Target in Osteoarthritis. *Curr Opin Rheumatol* **16**:616-622.

Busby WF, Jr., Ackermann J M and Crespi C L (1999) Effect of Methanol, Ethanol, Dimethyl Sulfoxide, and Acetonitrile on in Vitro Activities of CDNA-Expressed Human Cytochromes P-450. *Drug Metab Dispos* **27**:246-249.

Chauret N, Gauthier A and Nicoll-Griffith D A (1998) Effect of Common Organic Solvents on in Vitro Cytochrome P450-Mediated Metabolic Activities in Human Liver Microsomes. *Drug Metab Dispos* **26**:1-4.

Davies B and Morris T (1993) Physiological Parameters in Laboratory Animals and Humans. *Pharm Res* **10**:1093-1095.

Hall SD, Thummel K E, Watkins P B, Lown K S, Benet L Z, Paine M F, Mayo R R, Turgeon D K, Bailey D G, Fontana R J and Wrighton S A (1999) Molecular and Physical Mechanisms of First-Pass Extraction. *Drug Metab Dispos* **27**:161-166.

Hommes D, van den B B, Plasse T, Bartelsman J, Xu C, Macpherson B, Tytgat G, Peppelenbosch M and Van D S (2002) Inhibition of Stress-Activated MAP Kinases Induces Clinical Improvement in Moderate to Severe Crohn's Disease. *Gastroenterology* **122**:7-14.

Houston JB (1994) Utility of in Vitro Drug Metabolism Data in Predicting in Vivo Metabolic Clearance. *Biochem Pharmacol* **47**:1469-1479.

Hynes J, Jr. and Leftheri K (2005) Small Molecule P38 Inhibitors: Novel Structural Features and Advances From 2002-2005. *Curr Top Med Chem* **5**:967-985.

Kammerer, B., Scheible, H., Zurek, G., Godejohann, M., Zeller, K. P., Gleiter, C. H., Albrecht, W., and Laufer, S. Structural Elucidation of Metabolites of ML3403, a 4-pyridinylimidazole-type p38 MAP kinase inhibitor by LC-Qq-TOF-MS and LC-SPE-cryo-NMR/MS. Accepted in *Xenobiotica* 2007.

Kolars JC, Schmiedlin-Ren P, Schuetz J D, Fang C and Watkins P B (1992) Identification of Rifampin-Inducible P450IIIA4 (CYP3A4) in Human Small Bowel Enterocytes. *J Clin Invest* **90**:1871-1878.

Laufer SA, Wagner G K, Kotschenreuther D A and Albrecht W (2003) Novel Substituted Pyridinyl Imidazoles As Potent Anticytokine Agents With Low Activity Against Hepatic Cytochrome P450 Enzymes. *J Med Chem* **46**:3230-3244.

Natarajan SR and Doherty J B (2005) P38 MAP Kinase Inhibitors: Evolution of Imidazole-Based and Pyrido-Pyrimidin-2-One Lead Classes. *Curr Top Med Chem* **5**:987-1003.

Newton R and Holden N (2003) Inhibitors of P38 Mitogen-Activated Protein Kinase: Potential As Anti-Inflammatory Agents in Asthma? *BioDrugs* **17**:113-129.

Obach RS, Baxter J G, Liston T E, Silber B M, Jones B C, MacIntyre F, Rance D J and Wastall P (1997) The Prediction of Human Pharmacokinetic Parameters From Preclinical and in Vitro Metabolism Data. *J Pharmacol Exp Ther* **283**:46-58.

Pang KS and Rowland M (1977) Hepatic Clearance of Drugs. I. Theoretical Considerations of a "Well-Stirred" Model and a "Parallel Tube" Model. Influence of Hepatic Blood Flow, Plasma and Blood Cell Binding, and the Hepatocellular Enzymatic Activity on Hepatic Drug Clearance. *J Pharmacokinet Biopharm* **5**:625-653.

Peifer C, Wagner G and Laufer S (2006) New Approaches to the Treatment of Inflammatory Disorders Small Molecule Inhibitors of P38 MAP Kinase. *Curr Top Med Chem* **6**:113-149.

Ripp SL, Itagaki K, Philpot R M and Elfarra A A (1999) Species and Sex Differences in Expression of Flavin-Containing Monooxygenase Form 3 in Liver and Kidney Microsomes. *Drug Metab Dispos* **27**:46-52.

Rodrigues AD (1999) Integrated Cytochrome P450 Reaction Phenotyping: Attempting to Bridge the Gap Between CDNA-Expressed Cytochromes P450 and Native Human Liver Microsomes. *Biochem Pharmacol* **57**:465-480.

Tracy TS and Hummel M A (2004) Modeling Kinetic Data From in Vitro Drug Metabolism Enzyme Experiments. *Drug Metab Rev* **36**:231-242.

Wadsworth SA, Cavender D E, Beers S A, Lalan P, Schafer P H, Malloy E A, Wu W, Fahmy B, Olini G C, Davis J E, Pellegrino-Gensey J L, Wachter M P and Siekierka J J (1999) RWJ 67657, a Potent, Orally Active Inhibitor of P38 Mitogen-Activated Protein Kinase. *J Pharmacol Exp Ther* **291**:680-687.

Wagner G and Laufer S (2006) Small Molecular Anti-Cytokine Agents. *Med Res Rev* **26**:1-62.

Ward KW, Proksch J W, Azzarano L M, Mumawa J A, Roethke T J, Stelman G J, Walsh M J, Zeigler K S, McSurdy-Freed J E, Kehlert J R, Chokshi J, Levy M A and Smith B R (2001) Preclinical Pharmacokinetics of SB-203580, a Potent Inhibitor of P38 Mitogen-Activated Protein Kinase. *Xenobiotica* **31**:783-797.

Ward KW, Proksch J W, Gorycki P D, Yu C P, Ho M Y, Bush B D, Levy M A and Smith B R (2002a) SB-242235, a Selective Inhibitor of P38 Mitogen-Activated Protein Kinase. II: in Vitro and in Vivo Metabolism Studies and Pharmacokinetic Extrapolation to Man
3. *Xenobiotica* **32**:235-250.

Ward KW, Proksch J W, Salyers K L, Azzarano L M, Morgan J A, Roethke T J, McSurdy-Freed J E, Levy M A and Smith B R (2002b) SB-242235, a Selective Inhibitor of P38 Mitogen-Activated Protein Kinase. I: Preclinical Pharmacokinetics. *Xenobiotica* **32**:221-233.

Footnotes

B.K. and H.S. contributed equally to this work.

Figure legends:

Figure 1: Structures of ML3403 and ML3603 with IUPAC nomenclature

Figure 2: Metabolic profile of ML3403 with enzymes involved in the biotransformation

Figure 3: Percentage of metabolic conversion to ML3603 and M-sulfone after 10 min related to the ML3403 quantity at time t = 0 min (no conversion)

Figure 4: Relative product formation of M-421-pyr in male and female HLM and different rCYP isoenzymes

Figure 5: Kinetics of ML3403 sulfoxidation in female and male human liver microsomes and cDNA-expresssed isoenzymes (Values represent the mean ± S.E. of an experiment performed either in triplicate or duplicate for the rCYPs)

Figure 6: Mean plasma concentration/time profiles of ML3403 and its main metabolite ML3603 in male and female Wistar rats after oral administration of 30 mg/kg ML3403
(Values represent the mean with Error Bars (+ SD))

Figure 7: UV (320 nm), Base Peak (BPC) and Extracted Ion (EIC) chromatograms of a rat plasma sample (t = 2 h) and corresponding MS/MS-spectra of M-317, M-331 and M-345 and proposed fragment ions and structures

Table 1: Michaelis-Menten parameters by product formation and total normalized rates (%TNR) of the sulfoxidation

Species (Gender)	**K_{mapp}**	**V_{max}**			
	µM	pmol/min/mg			
HLM	2.3	111.0			
HLM (female)	1.3	87.7			
HLM (male)	1.7	61.7			
Isoenzyme	µM	pmol/min/pmol CYP	pmol CYP/mg*	pmol/min/mg	% TNR
CYP1A2	1.9	29.0	45	1305	32
CYP2C19	0.7	5.6	19	106	3
CYP2D6	14.4	63.7	10	637	15
CYP3A4	0.7	18.7	108	2024	50
			Total	4072	

*Nominal specific content of individual CYP proteins in native human liver microsomes (Gentest Corp.) (Rodrigues, 1999)

Table 2: Predictions of CL_{int} and CL_p from disappearance rates of ML3403 in liver microsomes from different species

Species	**Gender-specifity**	***in vitro* t½**	**CL_{int}**	**CL_{int}**	**$CL_{p\ well\ stirred}$**	**$CL_{p\ parallel\text{-}tube}$**
		[min]	µl/ (min*mg protein)	ml/ (min*kg body weight)	ml/ (min*kg body weight)	ml/ (min*kg body weight)
Mouse		5.9	472.5	1860.5	85.9	90.0
Rat		11.4	244.0	439.3	49.0	55.2
Rat	**female**	166.2	16.7	30.0	19.5	23.2
Rat	**male**	9.3	298.1	536.6	50.1	55.2
Monkey		47.6	58.2	78.6	28.0	36.4
Human		32.7	84.9	98.2	17.1	20.5
Human	**female**	29.6	93.6	108.2	17.4	20.6
Human	**male**	47.8	58.0	67.1	15.8	19.9

DMD Fast Forward. Published on March 7, 2007 as DOI: 10.1124/dmd.106.013409
This article has not been copyedited and formatted. The final version may differ from this version.

Table 3: Calculated pharmacokinetic parameters of ML3403 and ML3603 in Wistar rats, derived by non-compartmental analysis of mean concentration/time profiles after oral dosage

Compound	Gender	C_{max} [ng/ml]	t_{max} [h]	AUC_{0-t} [ng*h/ml]	λ_z [1/h]	$t_{½}$ [h]	$AUC_{0-\infty}$ [ng*h/ml]
ML3403	female	386	1.0	1479	0.16	4.3	1492
	male	115	1.0	398	0.31	2.3	409
ML3603	female	1123	1.0	4716	0.15	4.6	4742
	male	440	1.0	1344	0.51	1.4	1350

DMD Fast Forward. Published on March 7, 2007 as DOI: 10.1124/dmd.106.013409
This article has not been copyedited and formatted. The final version may differ from this version.

Table 4: Converted pharmacokinetic parameters C_{max} and AUC_{0-t} of ML3403 and ML3603 in rats and calculated ratios (female/male)

	female	male	**ratio (female/male)**
ML3403			
C_{max} [µM]	0.92	0.27	**3.36**
AUC_{0-t} [µM*h]	3.52	0.95	**3.72**
ML3603			
C_{max} [µM]	2.67	1.05	**2.55**
AUC_{0-t} [µM*h]	11.21	3.20	**3.51**
ML3403+ML3603			
C_{max} [µM]	3.59	1.32	**2.72**
AUC_{0-t} [µM*h]	14.73	4.14	**3.56**

Table 5: Compilation of the identified metabolites and ML3403 with their characteristics

		RT [min]	$[M+H]^+$	Main fragment ions m/z measured	Phenylethyl moiety	Proposed structural elements	Major responsible P-450 isoenzymes/ transferases
Phase I metabolites	**M-317**	13.1	317.1	302, 269, 253, 213	removed	sulfoxide / $-NH_2$	3A4
	M-333	13.4	333.1	253, 213	removed	sulfone / $-NH_2$	1A2
	M-301	13.9	301.1	286, 285, 268, 253, 227	removed	sulfide / $-NH_2$	3A4
	M-437-121	14.1	437.1	317, 302, 299, 121	oxidized	sulfoxide + [O]	2C19
	ML3603	15.3	421.1	406, 317, 302, 253, 105	unmodified	sulfoxide	3A4 >1A2 > 2D6 > 2C19
	M-sulfone	16.5	437.1	333, 318, 105	unmodified	sulfone	1A2
	ML3403	18.6	405.1	301, 286, 285, 253, 105	unmodified	sulfide	---
	M-421-pyr	23.8	421.1	317, 300, 299, 267, 105	unmodified	pyridine-N-oxide	3A4
	M-437-pyr	20.5	437.1	333, 318, 301, 105	unmodified	pyridine-N-oxide sulfoxide	3A4
Phase II metabolites	**M-331**	13.3	331.1	316, 283, 267, 227	removed N conjugated	sulfoxide / $-NH_2$ + methyl-amine	N-methyltransferase (NMT)
	M-345	13.4	345.1	330, 297, 281, 241	removed N conjugated	sulfoxide / $-NH_2$ + dimethyl-amine	N-methyltransferase (NMT)
	M-359	14.0	359.1	344, 302, 285, 253	removed N conjugated	sulfoxide / $-NH_2$ + acetyl-amine	N-acetyltransferase (NAT)
	M-361	13.7	361.1	281, 253, 241	removed N conjugated	sulfone / $-NH_2$ + dimethyl-amine	N-methyltransferase (NMT)

Figure 1

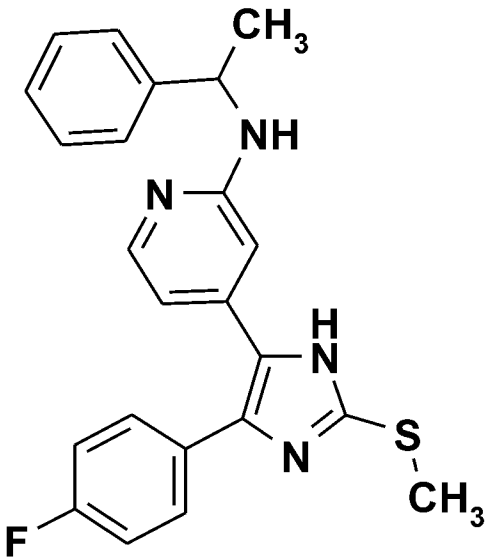

ML3403:
{4-[5-(4-Fluoro-phenyl)-2-methylsulfanyl-3H-imidazol-4-yl]-pyridin-2-yl}-(1-phenyl-ethyl)-amine

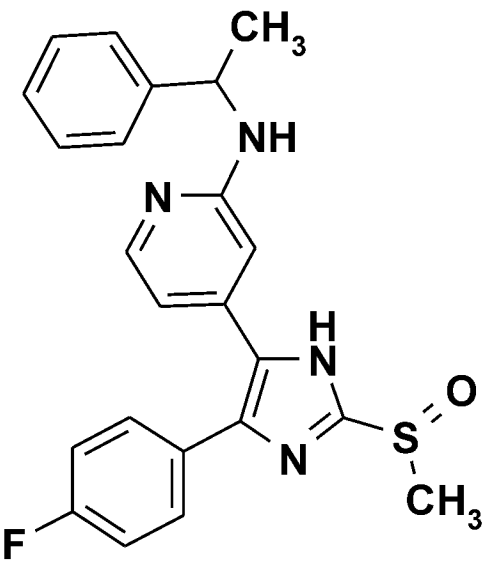

ML3603:
{4-[5-(4-Fluoro-phenyl)-2-methanesulfinyl-3H-imidazol-4-yl]-pyridin-2-yl}-(1-phenyl-ethyl)-amine

Figure 2

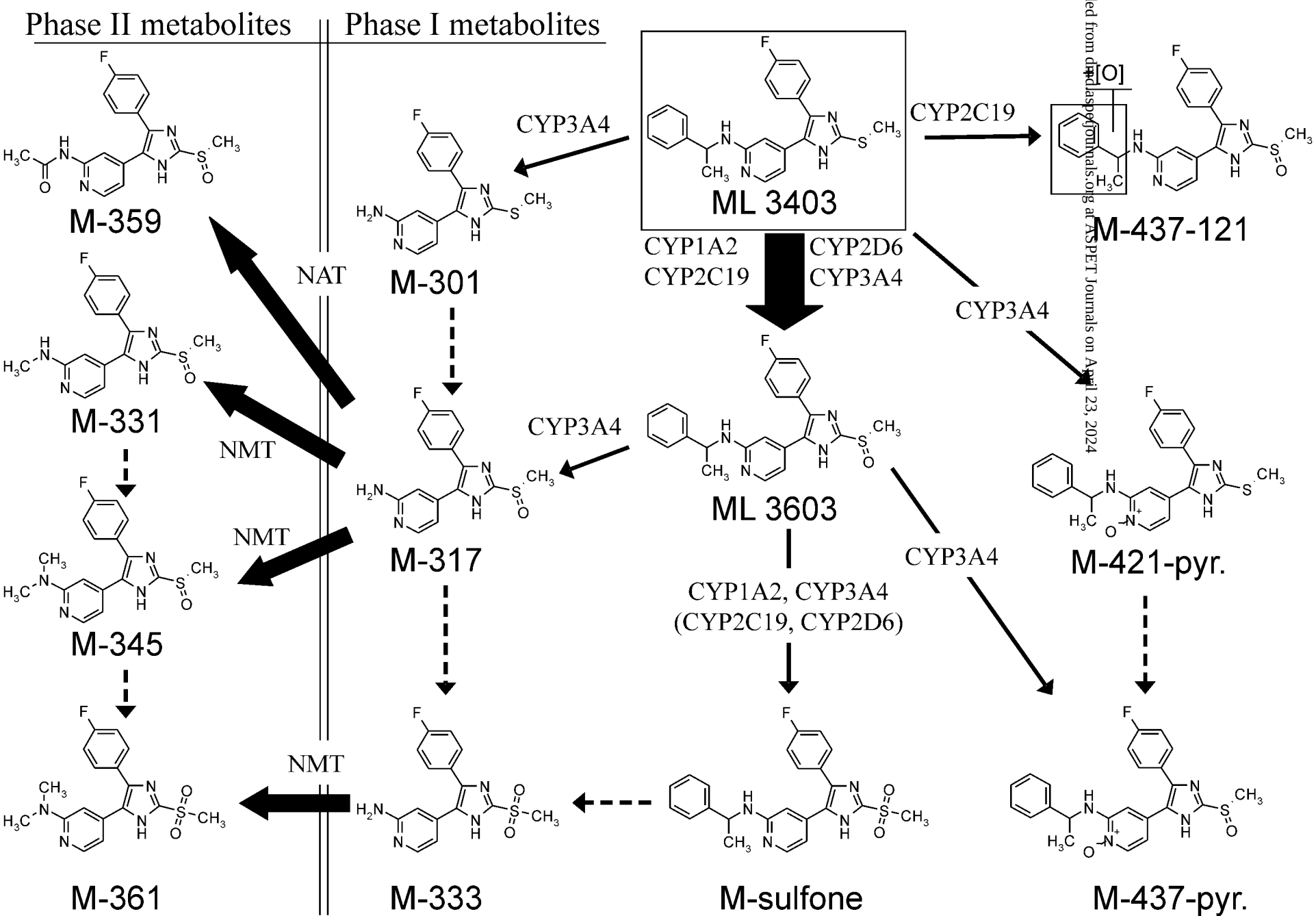

Figure 3

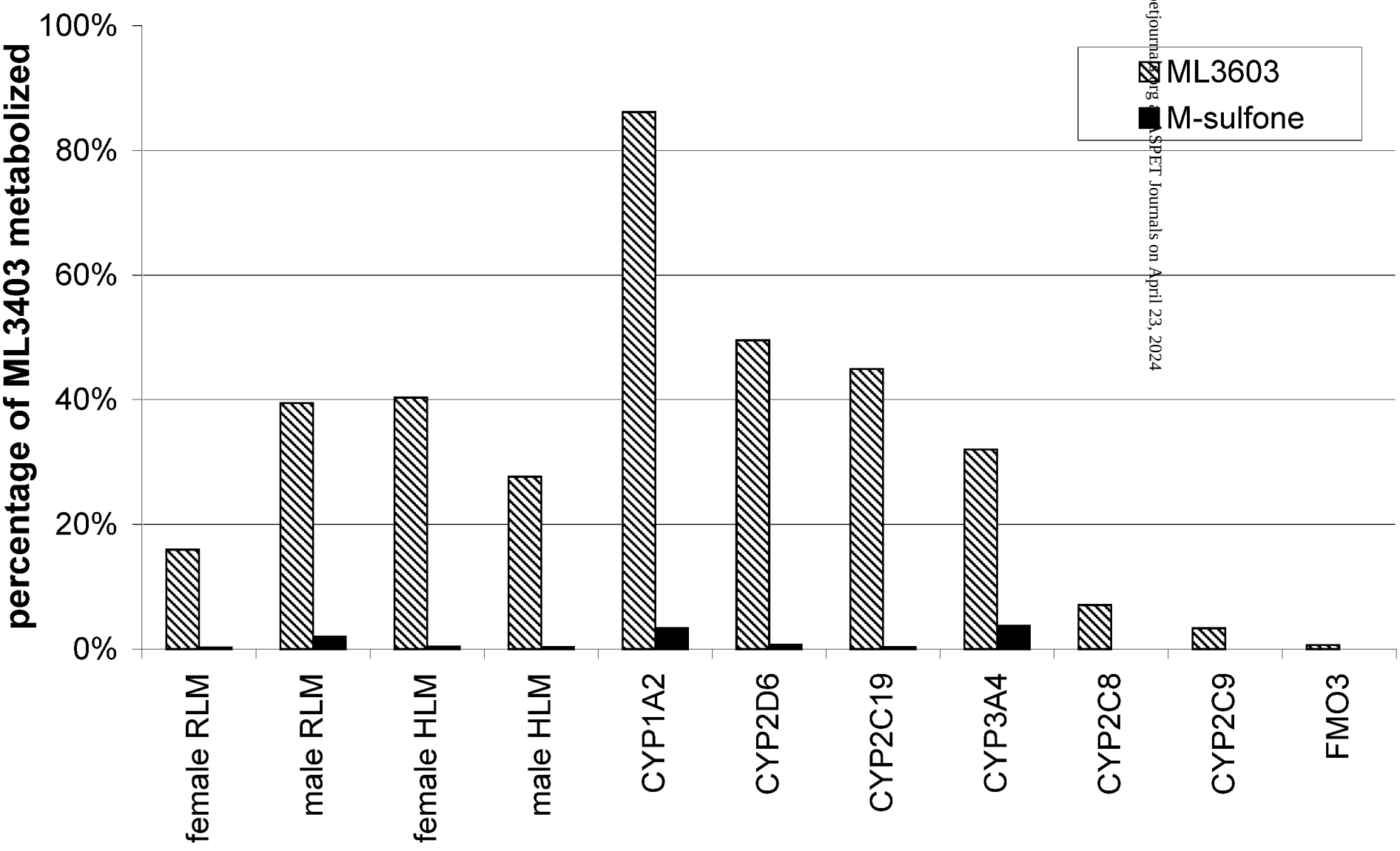

Figure 4

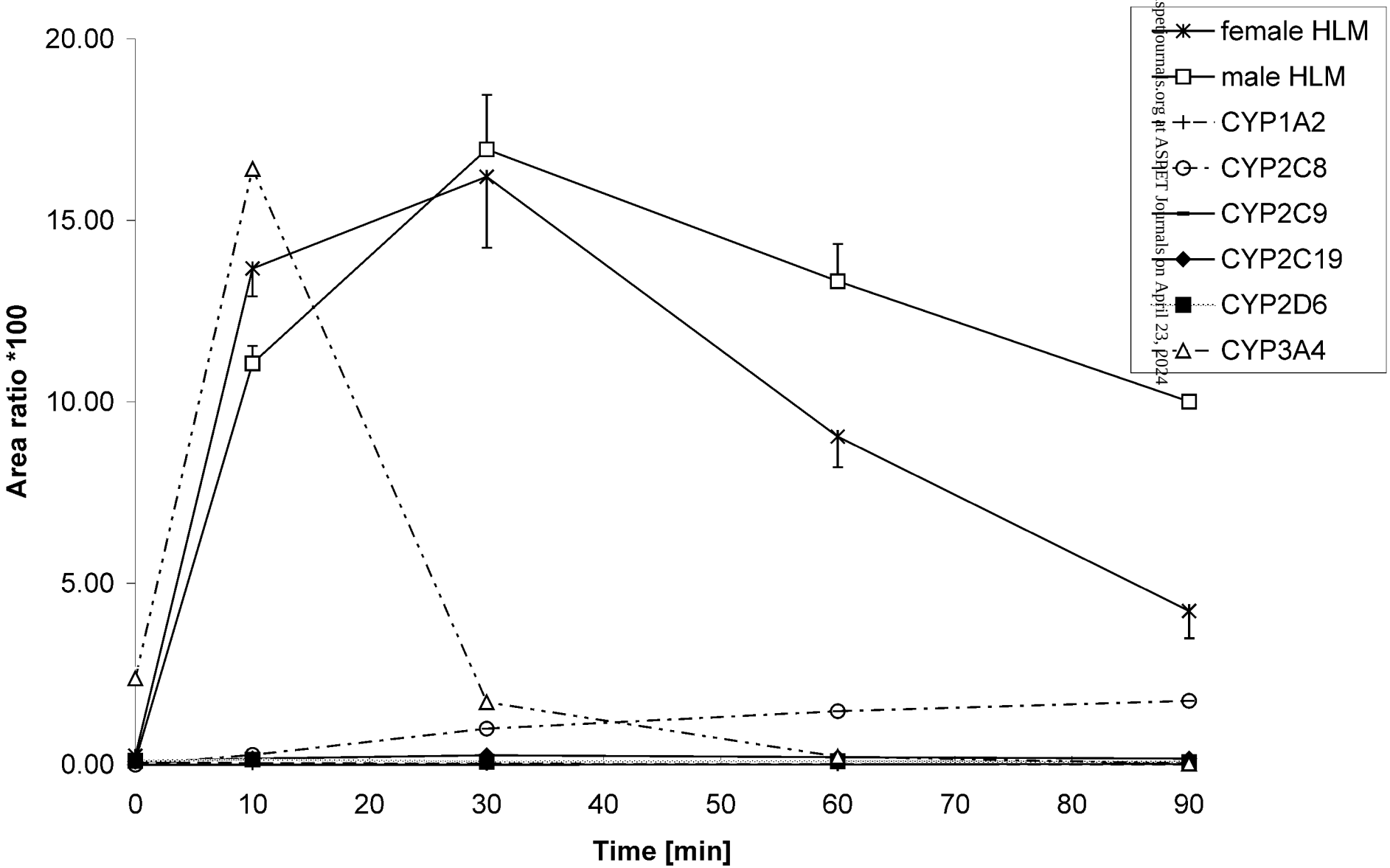

Figure 5

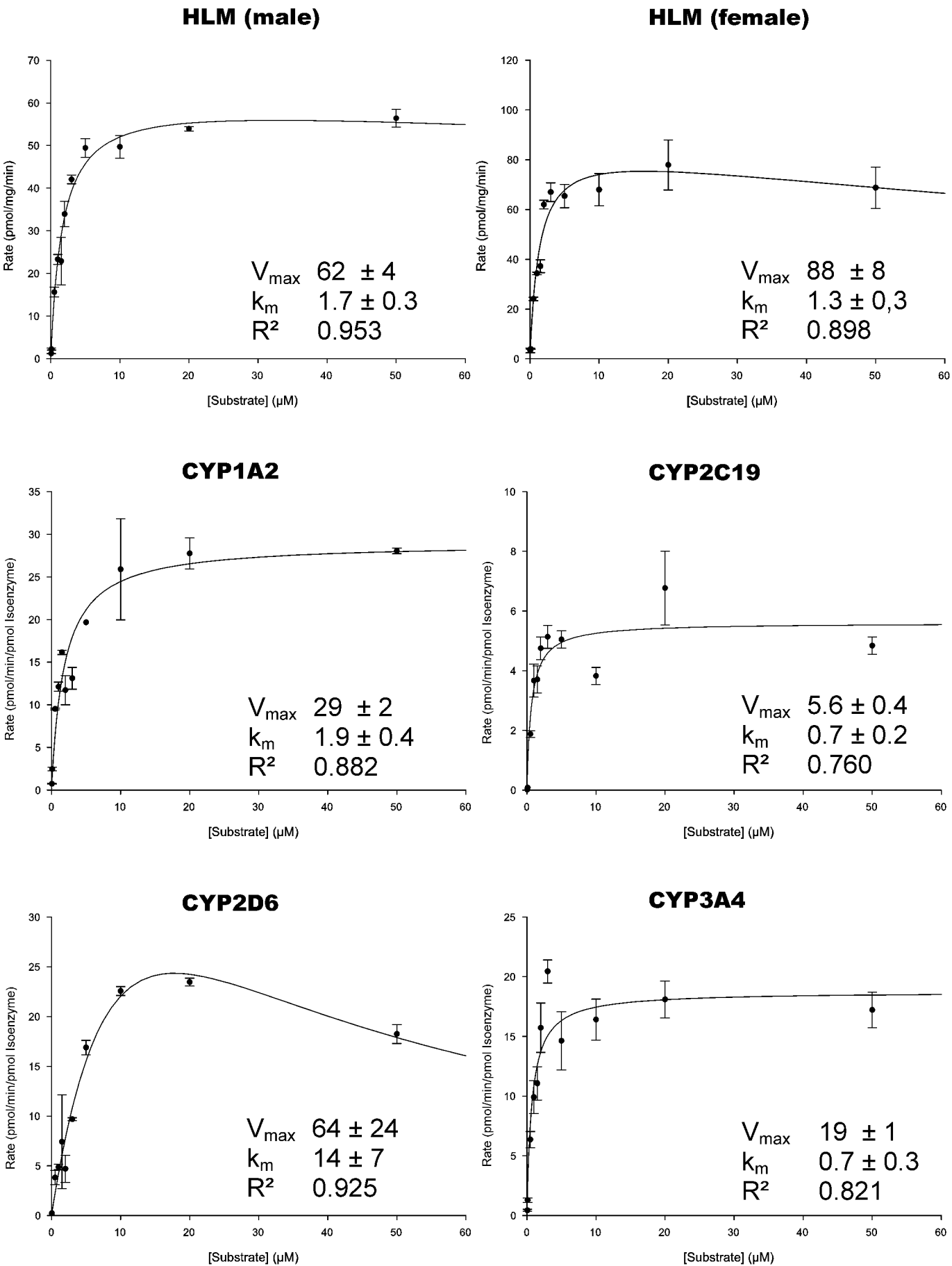
HLM (male)
Rate (pmol/mg/min)
[Substrate] (μM)
Vmax 62 ± 4
km 1.7 ± 0.3
R² 0.953
HLM (female)
Rate (pmol/mg/min)
[Substrate] (μM)
Vmax 88 ± 8
km 1.3 ± 0,3
R² 0.898
CYP1A2
Rate (pmol/min/pmol Isoenzyme)
[Substrate] (μM)
Vmax 29 ± 2
km 1.9 ± 0.4
R² 0.882
CYP2C19
Rate (pmol/min/pmol Isoenzyme)
[Substrate] (μM)
Vmax 5.6 ± 0.4
km 0.7 ± 0.2
R² 0.760
CYP2D6
Rate (pmol/min/pmol Isoenzyme)
[Substrate] (μM)
Vmax 64 ± 24
km 14 ± 7
R² 0.925
CYP3A4
Rate (pmol/min/pmol Isoenzyme)
[Substrate] (μM)
Vmax 19 ± 1
km 0.7 ± 0.3
R² 0.821

Figure 6

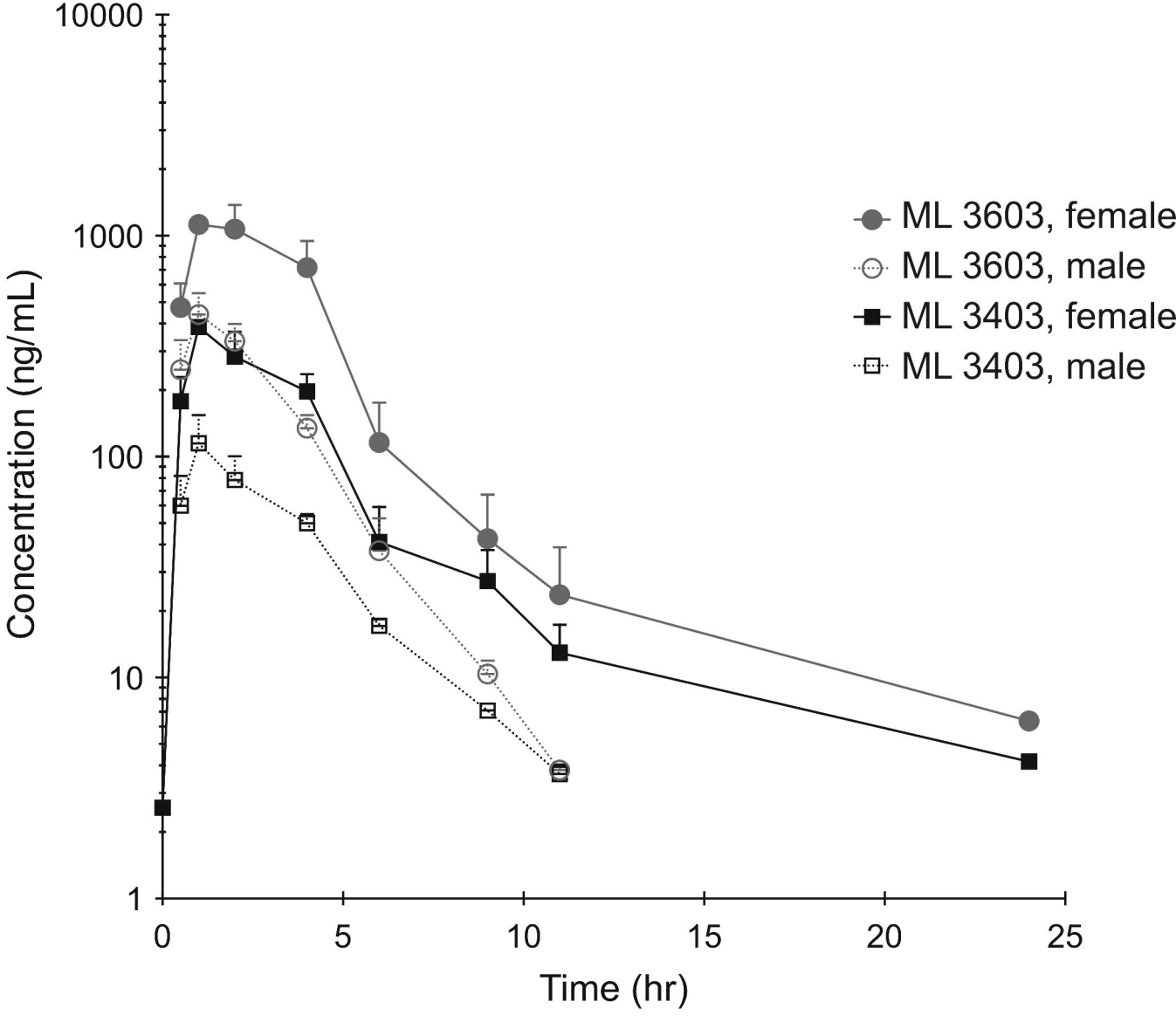
10000
1000
100
10
1
Concentration (ng/mL)
0
5
10
15
20
25
Time (hr)
ML 3603, female
ML 3603, male
ML 3403, female
ML 3403, male

Figure 7